

**From multifragmentation to neck fragmentation: Mass, isospin, and velocity correlations**V. Baran,<sup>1,\*</sup> M. Colonna,<sup>2</sup> M. Di Toro,<sup>2,3</sup> and R. Zus<sup>1</sup><sup>1</sup>*Physics Faculty, University of Bucharest, RO-77125 Bucharest, Romania*<sup>2</sup>*Laboratori Nazionali del Sud, Istituto Nazionale di Fisica Nucleare, I-95123 Catania, Italy*<sup>3</sup>*Physics and Astronomy Department, University of Catania, I-95124 Catania, Italy*

(Received 23 May 2011; revised manuscript received 27 March 2012; published 8 May 2012)

We present new features of fragmentation dynamics at the transition from semicentral to semiperipheral heavy-ion collisions at Fermi energies, as obtained within a microscopic transport model, the stochastic mean field. We show that, along this transition, specific hierarchy phenomena of some kinematic observables associated with the intermediate mass fragments develop. Their correlations with the dynamics of the isospin degree of freedom, predicted by our calculations, open new possibilities to learn about the density dependence of nuclear symmetry energy below saturation, as well as about the relevant fragmentation mechanisms. Detailed results are presented for mass symmetric Sn + Sn reactions with different isospin content at 50 MeV/nucleon.

DOI: [10.1103/PhysRevC.85.054611](https://doi.org/10.1103/PhysRevC.85.054611)

PACS number(s): 25.70.Pq, 25.70.Mn, 21.65.Ef, 24.10.Cn

**I. INTRODUCTION**

Nucleus-nucleus collisions provide a unique tool to explore the properties of finite interacting fermionic systems in a broad range of densities and temperatures. At energies between 10 and 100 MeV/nucleon, usually referred to as *Fermi energies*, the mean-field and collisional effects are quite balanced, leading to a very intricate dynamics, sensitive to impact parameter and beam energy. Entrance channel effects, as well as phenomena well explained in terms of statistical equilibrium, can coexist. Moreover, as a consequence of the two-component character of nuclear matter, additional features due to isospin manifest. The symmetry energy term in the equation of state (EOS) was one of the main subjects of interest during the last decade [1–3].

The fragmentation process is a ubiquitous phenomenon observed at Fermi energies. However, the underlying reaction mechanisms can be rather different and a detailed study can provide independent information on the nuclear EOS out of saturation. The aim of this paper is to suggest new fragment mass-velocity-isospin correlations particularly sensitive to the fragmentation mechanism, as well as to the in-medium nuclear interaction.

For central collisions, the nuclear multifragmentation can be associated with a liquid-gas phase transition in a composite system [4]. While the final-state configurations are well described within statistical equilibrium models [5–8], but also within hybrid models coupling a dynamical formation and evolution of primary fragments with a secondary decay stage [9], the kinetics of this phase transition can be related to spinodal decomposition in two-component nuclear matter [4,10,11] accompanied by the isospin distillation. For semiperipheral collisions, the neck fragmentation with a peculiar intermediate mass fragment (IMF,  $3 \leq Z \leq 20$ ) distribution and an entrance channel memory was observed experimentally [12–17] and predicted by various transport models [18–20]. In this case, the low-density neck region triggers an isospin migration from

the higher density regions corresponding to the projectilelike fragment (PLF) and targetlike fragment (TLF). Therefore, the isospin content of the IMF's is expected to reflect the isospin enrichment of the midvelocity region. For even more peripheral collisions, an essentially binary reaction in the exit channel can be accompanied by a dynamically induced fission of the participants [21–23], and for  $N/Z$ -asymmetric entrance channel combinations isospin diffusion drives the system toward charge equilibration [24–27].

Consequently, the isospin degree of freedom can be seen as a precious tracer providing additional information about the physical processes taking place during the evolution of the colliding systems. Moreover, from a comparison between the experimental data and the theoretical model predictions, isospin dynamics allows one to investigate the density and/or temperature dependence of the symmetry energy. More exclusive analyzes from the new experimental facilities will certainly impose severe restrictions on various models and parametrizations concerning this quantity.

The purpose of this article is to perform a detailed investigation of the fragmentation dynamics at the transition from semicentral to semiperipheral collisions, a region not much studied until now and which can be identified in modern experiments. An interplay between statistical and dynamical mechanisms is expected and we clearly evidence the development of hierarchy effects in the transverse velocity of IMF's. Moreover, new interesting correlations between kinematic features of the fragments and isospin dynamics, which can provide clues in searching for the most sensitive observables to the symmetry energy, are noted. We mention that for central collisions a radial expanding multifragmenting source develops, and a correlation between fragment  $N/Z$  and kinetic energy, sensitive to the density behavior of the symmetry energy, was recently discussed in a transport model [28]. The average value of this ratio decreases with the kinetic energy per nucleon and it is asy-EOS dependent.

We also mention that, in an experimental study of internal correlations for the fragmentation of quasiprojectiles performed by Colin *et al.* [29] within the INDRA collaboration, for certain classes of events, a hierarchy of mass

\*baran@nipne.ro

fragments along the beam axis was interpreted in terms of the breakup of the very elongated structure emerging from the interaction of the two colliding nuclei. More recently, McIntosh *et al.* [30] examined the fragment emission from Xe + Sn peripheral and midperipheral dissipative collisions. A significant enhancement of backward fragments yield relative to the forward component as well as an alignment with the direction of projectilelike residue velocity were evidenced. Therefore it is interesting to understand how these dynamical effects evolve for even more dissipative processes.

In Sec. II we briefly review the transport approach and specify the reactions which are studied. Section III is focused on the properties of the observed fragmentation mechanisms. Isospin effects are analyzed in Sec. IV in connection with the kinematic features of the fragments. Finally, in Sec. V the conclusions and some suggestions for experiments are presented.

## II. TRANSPORT APPROACH

Our analysis is performed within a semiclassical microscopic transport model, the stochastic mean field (SMF), based on the Boltzmann-Nordheim-Vlasov equation [4]. Our choice is motivated by the requirement to have a well-implemented nuclear mean-field dynamics together with the effects of fluctuations induced by two-body scatterings. Experimental indications at energies between 20 and 100 MeV/nucleon, including the behavior of collective flows, suggest that mean field plays an essential role in shaping the evolution of the system. Within the SMF model, the time evolution of the one-body distribution function  $f(\mathbf{r}, \mathbf{p}, t)$  is described by a Boltzmann-Langevin equation [31]:

$$\frac{\partial f}{\partial t} + \frac{\mathbf{p}}{m} \frac{\partial f}{\partial \mathbf{r}} - \frac{\partial U}{\partial \mathbf{r}} \frac{\partial f}{\partial \mathbf{p}} = I_{\text{coll}}[f] + \delta I[f], \quad (1)$$

where the fluctuating term  $\delta I[f]$  is implemented through stochastic spatial density fluctuations [32]. The average collision integral  $I_{\text{coll}}[f]$  for fermionic systems takes into account the energy and the angular and isospin dependence of free nucleon-nucleon cross sections.

We adopted the following parametrization of the mean-field potential:

$$U_q = A \frac{\rho}{\rho_0} + B \left( \frac{\rho}{\rho_0} \right)^{\alpha+1} + C(\rho) \frac{\rho_n - \rho_p}{\rho_0} \tau_q + \frac{1}{2} \frac{\partial C}{\partial \rho} \frac{(\rho_n - \rho_p)^2}{\rho_0}, \quad (2)$$

where  $q = n, p$ ,  $\tau_n = 1$ , and  $\tau_p = -1$ . The coefficients  $A = -356.8$  MeV and  $B = 303.9$  MeV and the exponent  $\alpha = \frac{1}{6}$ , characterizing the isoscalar part of the mean field, are fixed, requiring that the saturation properties of symmetric nuclear matter,  $\rho_0 = 0.16$  fm<sup>-3</sup> and  $E/A = -16$  MeV/nucleon, with a compressibility around 200 MeV, are reproduced. This choice corresponds to a Skyrme-like effective interaction, namely, SKM\*, for which we consider the effective mass as being equal to nucleon bare mass,  $m = 938$  MeV/c<sup>2</sup>. Following our previous work [33], the symmetry energy effects were studied by employing two different density parametrizations of the symmetry potential, named *asyssoft*

and *asysuperstiff*. For *asyssoft* EOS,  $\frac{C(\rho)}{\rho_0} = 482 - 1638\rho$ , the potential part of the symmetry energy  $E_{\text{sym}}^{\text{pot}} = \frac{1}{2} C(\rho) \frac{\rho}{\rho_0}$  has a weak density dependence close to the saturation, being almost flat around  $\rho_0$ . For the *asysuperstiff* case,  $\frac{C(\rho)}{\rho_0} = \frac{32}{\rho_0} \frac{2\rho}{\rho + \rho_0}$ , the symmetry energy is quickly decreasing for densities below normal density.

Surface terms are not explicitly included in the mean-field potential, however surface effects are accounted for by considering finite width wave packets for the test particles employed in the numerical resolution of Eq. (1). The width is tuned to reproduce the surface energy of nuclei in the ground state [34]. This method also induces the presence of a surface term in the symmetry energy. We have checked that properties connected to surface effects, such as the neutron skin of neutron-rich nuclei, are in reasonable agreement with calculations of other models employing similar interactions [35,36].

A comparative study of the reactions <sup>124</sup>Sn+<sup>124</sup>Sn (Heavy-Heavy combination, HH) and <sup>112</sup>Sn+<sup>112</sup>Sn (Light-Light combination, LL) at 50A MeV is performed. These combinations were intensively analyzed in recent years at Michigan State University, (MSU) [24]. We shall focus on the value of impact parameter  $b = 4$  fm, for which a typical behavior, corresponding to the transition from multifragmentation to neck fragmentation, is clearly noted in our simulations. Indeed, our previous results for these systems indicate that for central collisions, corresponding to impact parameters until 2–3 fm, after a compression stage an expansion takes place plugging the system at densities below saturation and driving the fragment formation and growth. This takes place until a freeze-out configuration is attained, corresponding to a saturation of the number of produced IMF's. The corresponding time scales are of the order of 300–350 fm/c for these phases of the reaction. On the other hand, around  $b = 6$  fm the reaction mechanism corresponds to a neck fragmentation with mostly two or three IMF's observed in the midrapidity region and a short nucleus-nucleus interaction time, below 120–130 fm/c.

For an intermediate situation between the two scenarios presented above, at  $b = 4$  fm for instance, a memory of the entrance channel is kept, through the existence of well-defined PLF's and TLF's, but the multiplicity of intermediate mass fragments is still quite large [37]. These features are depicted in Fig. 1, where the density contour plots in the reaction plane are displayed for the system <sup>124</sup>Sn+<sup>124</sup>Sn.

Therefore, along this transition region, for impact parameters between 3 and 5 fm, corresponding to a consistent reaction cross section, a mixing of features associated with multifragmentation and neck fragmentation is expected. The relative values of the interaction time (now of the order of 130–180 fm/c), of the time associated with fragment formation and growth, as well as of the time scales for isospin migration and distillation, will determine the properties of the emitted IMF's. Consequently, a good sensitivity to the symmetry energy density dependence can show up.

## III. FRAGMENTATION MECHANISM

A total number of 2000 events is generated for each entrance channel combination and equation of state at impact parameter  $b = 4$  fm.

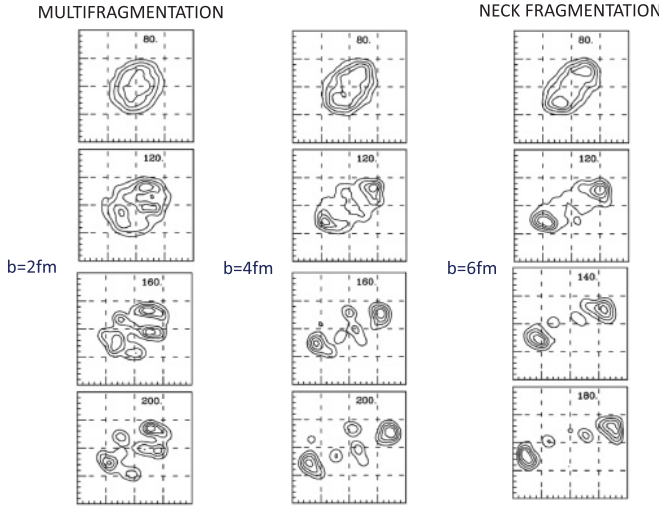


FIG. 1. (Color online) Density contour plots on the reaction plane ( $xOz$ ,  $Oz$  is the beam axis), for the system  $^{124}\text{Sn} + ^{124}\text{Sn}$  at 50A MeV. Three impact parameters are considered, and the time scales in each box (of linear size 40 fm) are expressed in fm/c units.

First, we adopt an analysis method of kinematic properties previously employed in studies concerning dynamical fission or neck fragmentation mechanisms [38,39].

After the freeze-out time, corresponding to the saturation of the number of formed IMF's, we propagate the Coulomb trajectories of all fragments until a configuration where the Coulomb interaction becomes negligible. The asymptotic velocities of PLF and TLF define an intrinsic axis of the event by the vector  $\mathbf{V}_r = \mathbf{V}(H_1) - \mathbf{V}(H_2)$  always oriented from the second heaviest fragment  $H_2$  toward the heaviest one  $H_1$ . Even for mass symmetric entrance channels this is an appropriate definition when searching for the correlations between kinematic properties of the IMF's and the breakup of the initial composite system. At freeze-out time the IMF's of each event are ordered in mass. The orthogonal and parallel components of their asymptotic velocities with respect to the intrinsic axis,  $v_{\text{tra}}$  and  $v_{\text{par}}$ , respectively, together with their charge  $Z$ , are determined. The events are classified according to the number of observed IMF's at the freeze-out time. We report in Fig. 2 the fragments' multiplicity distributions associated with all cases investigated. It is observed that more neutron-rich systems favor larger IMF multiplicities. We select the classes with three IMF's (the total number of fragments  $N_F = 5$ ) and four IMF's ( $N_F = 6$ ), corresponding to around 550 events and 250 events out of the total of 2000 events, providing thus a reasonable statistics.

The charge distributions corresponding to each order in the mass hierarchy are shown in Fig. 3, for the events with three IMF's and all entrance channel combinations, HH and LL, respectively. The heaviest IMF (the rank one in the hierarchy) can have a charge up to  $Z = 16-18$  with distribution centered around  $Z = 6-8$  [see Figs. 3(a)-3(d), black solid line] while the lightest goes up to  $Z = 8$  [see the thin dotted line in Figs. 3(a)-3(d)]. In the bottom row of the figure is plotted the average transverse velocity in each charge bin calculated by considering all fragments independent of the position in the

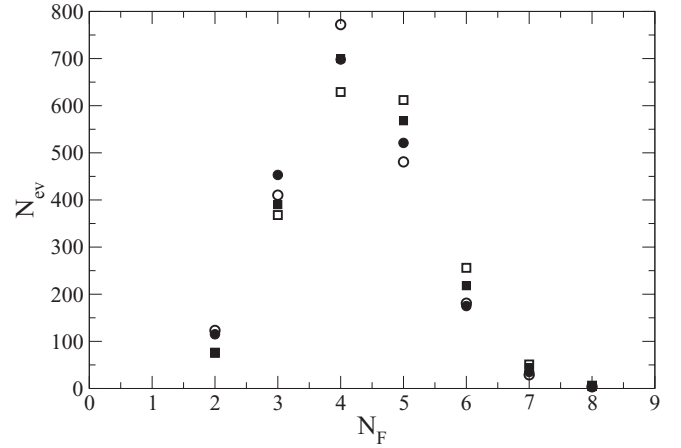


FIG. 2. Fragment multiplicity distribution at  $b = 4$  fm. Circles:  $^{112}\text{Sn} + ^{112}\text{Sn}$ . Squares:  $^{124}\text{Sn} + ^{124}\text{Sn}$ . Filled symbols: asysoft EOS. Open symbols: asysuperstiff EOS.

hierarchy [see Fig. 3(e) and 3(f)]. The transverse velocity has a steep decreasing trend with the charge, in agreement with previous findings reported in [40], and does not depend much on the asy-EOS. In fact, this appears to be one feature of the fragmentation dynamics. The larger transverse velocity of the lightest fragments seems to indicate that this emission is not much influenced by the presence of the PLF, TLF "spectators." All these features can be related to the presence of a deformed multifragmenting source located in the overlap region upon which the shape instabilities of the neck dynamics will take over. These observations require a more detailed investigation

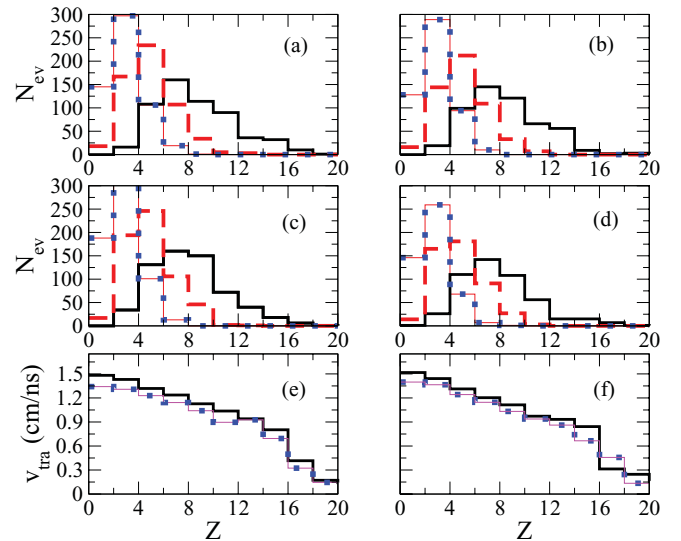


FIG. 3. (Color online) The charge distribution for each IMF in the hierarchy: asysoft EOS (upper row) and asysuperstiff EOS (middle row). (a, c, and e) HH combination. (b, d, and f) LL combination. Heaviest (black, continuous line), second heaviest (red, long-dashed line), and third heaviest (blue, dotted line) fragments in the hierarchy. Average transverse velocity distribution as a function of the charge (bottom row) for the asysoft EOS (thick solid line) and asysuperstiff EOS (thin dashed line). All results refer to events with IMF multiplicity equal to three.

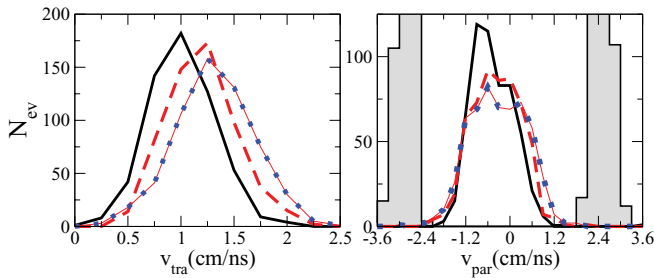


FIG. 4. (Color online) HH combination and the asysoft EOS choice. Fragmentation events with three IMFs. Left panel: transverse velocity  $v_{\text{tra}}$  distributions. Right panel: parallel velocity  $v_{\text{par}}$  distributions. Heaviest (black, continuous line), second heaviest (red, long-dashed line), and third heaviest (blue, dotted line) fragments in the hierarchy.

of the kinematic properties of fragments, once ordered in mass. As we shall see, the correlations between velocity and size are amplified when analyzing the events according to the fragment rank in the hierarchy.

Figures 4–7 show, for asysoft and asysuperstiff EOS, respectively, the IMF's transverse and parallel velocity distributions in the case of HH combination. We also report, for reference, the parallel velocity distributions of projectile- and targetlike residues as they result from our calculations at these energies.

The velocity distributions along the intrinsic axis (right panels) are centered around the midvelocity region, quite decoupled from PLF and TLF. This is analogous to what it is observed in neck fragmentation. The width of the distributions is essentially related to thermal fluctuations, being larger for the lightest IMF's, as expected.

We notice that, for both classes of events considered (with three and four IMF's), the transverse velocity distribution shifts toward higher values with the IMF position in the mass hierarchy, the lightest fragment acquiring the greatest  $v_{\text{tra}}$ . This hierarchy in the velocity perpendicular to the intrinsic axis emerges as a specific signal characterizing the transition from multifragmentation to neck fragmentation. It can be related to the peculiar geometrical configuration of the overlapping

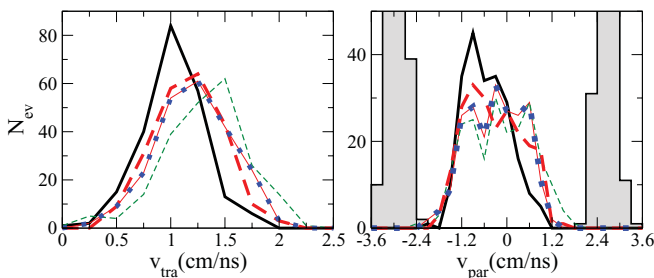


FIG. 5. (Color online) HH combination and the asysoft EOS choice. Fragmentation events with four IMF's. Left panel: transverse velocity  $v_{\text{tra}}$  distributions. Right panel: parallel velocity  $v_{\text{par}}$  distributions. Heaviest (black, continuous line), second heaviest (red, long-dashed line), and third heaviest (blue, dotted-line) and the lightest (green, short-dashed line) IMF's in the hierarchy.

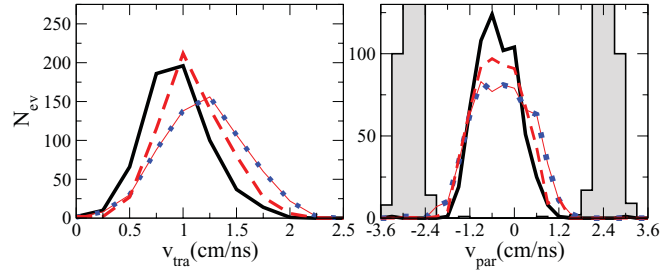


FIG. 6. (Color online) Like Fig. 4, for the asysuperstiff EOS choice.

region and its fast evolution at these impact parameters, as will be better explained in the following.

We studied the transverse velocity features in more detail, by looking separately at in reaction and out of reaction plane components,  $v_{\text{tra}x}$  and  $v_{\text{tra}y}$  (see Figs. 8 and 9). For both quantities we notice an interesting correlation to the fragment position in the hierarchy. Heavier fragment distributions are peaked at a larger velocity  $v_{\text{tra}y}$  in the out-of-plane direction (right panels), as a result of the stronger Coulomb repulsion. On the other hand, due to the balance between Coulomb forces exerted by PLF and TLF, the in-plane distribution is peaked at a transverse velocity close to zero. Increasing the rank of the hierarchy, interesting effects are observed for the in-plane transverse velocity distributions: these are shifted toward higher velocities for lighter fragments (left panels). This effect can be attributed to the development of a collective flow, similar to the radial flow observed in central multifragmentation events, that emerges mostly along the in-plane transverse direction, reflecting the geometrical configuration of the events considered in our analysis. This scenario is consistent with the formation of light fragments via a faster multifragmentation mechanism, while heavier masses are formed on longer time scales, when the initial collective energy has been dissipated. We notice that, when the two components are combined to generate the final transverse velocity distributions, the hierarchy signal still remains rather robust (see Figs. 4–7).

It is worth mentioning that, due to the lack of fluctuations in full momentum space, average fragment kinetic energies are underestimated in the SMF model. This amounts to a 20% effect for reactions in the beam energy range considered here [41]. We consider this limit as quite acceptable, taking into account that the transport model is able to provide

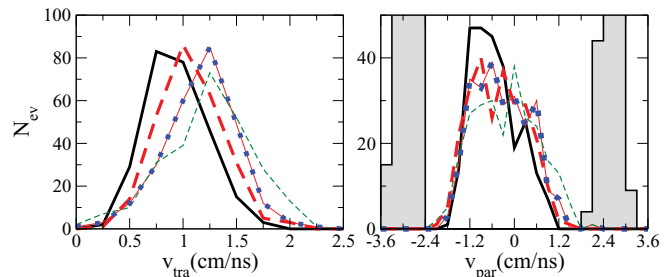


FIG. 7. (Color online) Like Fig. 5, for the asysuperstiff EOS choice.

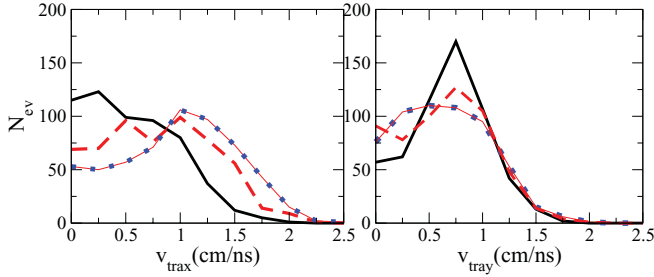


FIG. 8. (Color online) HH combination and the asysoft EOS. Left panel: transverse velocity in reaction plane distribution for fragmentation events with three IMF's. Right panel: transverse velocity out of reaction plane distribution for fragmentation events with three IMF's. All lines are as in the caption of Fig. 4.

a self-consistent and realistic description of the evolution from the entrance to the exit channel, without any additional ingredients or assumptions. However, this drawback does not affect the main results of our analysis, i.e., the presence of hierarchy effects in the fragment velocity distributions, clearly seen in Figs. 4–7. A quantitative reproduction of the transverse velocity distributions experimentally observed is beyond the scope of the present manuscript.

To gain more insight into the competition between thermal and dynamical, nonequilibrium effects, we analyzed the collective flow properties associated with the IMF's. For each rank in the mass hierarchy, the transverse and elliptic flow parameters were obtained as

$$v_1 = \left\langle \frac{p_x}{p_T} \right\rangle; \quad v_2 = \left\langle \frac{p_x^2 - p_y^2}{p_T^2} \right\rangle, \quad (3)$$

where  $p_x$  now refers to the in reaction plane component of the momentum perpendicular to the beam axis, while  $p_y$  is the momentum component orthogonal to the reaction plane. Here  $p_T = \sqrt{p_x^2 + p_y^2}$  is the transverse momentum and the average was performed over the number of events. The different behavior of the IMF's transverse velocity components, for various positions in the mass hierarchy discussed above, should be clearly distinguished in the flows.

In Fig. 10 we report the in-plane transverse flow  $v_1$  as a function of the fragment velocity along beam axis  $v_z$ , for

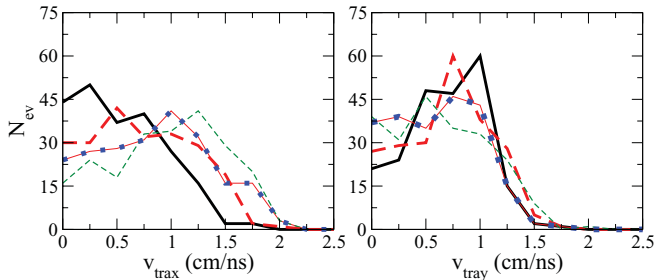


FIG. 9. (Color online) HH combination and the asysoft EOS. Left panel: transverse velocity in reaction plane distribution for fragmentation events with four IMF's. Right panel: transverse velocity out of reaction plane distribution for fragmentation events with four IMF's. All lines are as in the caption of Fig. 5.

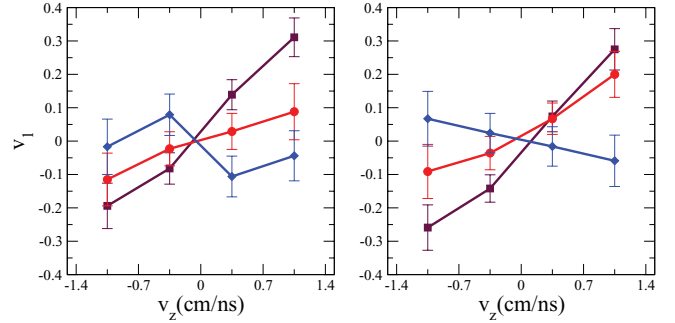


FIG. 10. (Color online) Direct flow parameter  $v_1$  as a function of velocity along beam axis  $v_z$ . HH combination and events with three IMF's. Squares: heaviest IMF. Circles: second heaviest IMF. Diamonds: lightest IMF in the hierarchy. Left panel: asysoft EOS. Right panel: asysuperstiff EOS.

each rank in the mass hierarchy, with three IMF's. The light fragments present an almost flat, close to zero transverse flow, fully consistent with an early formation and decoupling in the midrapidity zone. At variance, the heavy fragments nicely follow a positive or negative value due to the correlation to the PLF or TLF spectators. In Fig. 11 we represent the elliptic flow parameter  $v_2$  dependence on the total transverse velocity  $v_T = \sqrt{v_x^2 + v_y^2}$ , again for each of the three orders in the hierarchy. For small  $v_T$  the elliptic flow is negative, indicating a behavior dominated by the Coulomb repulsion out of reaction plane. However, the value of the anisotropy parameter  $v_2$  increases with the position in the hierarchy in a given bin of  $v_T$ . It also rises with the transverse velocity, becoming positive above  $v_T \approx 1.4$  cm/ns. This feature can be related to the incomplete dissipation of the entrance channel collective energy, driving the lighter fragments more easily on the reaction plane. We have to look at this figure also in connection to Fig. 3 (bottom panel), where the  $v_{tra}$  distribution versus charge is presented. Light fragments, more abundant at high transverse velocities, clearly show positive elliptic flow fully consistent with the analysis of Fig. 8. Heavier fragments, more abundant at lower  $v_{tra}$ , nicely show more negative  $v_2$  values, again in agreement with the results of

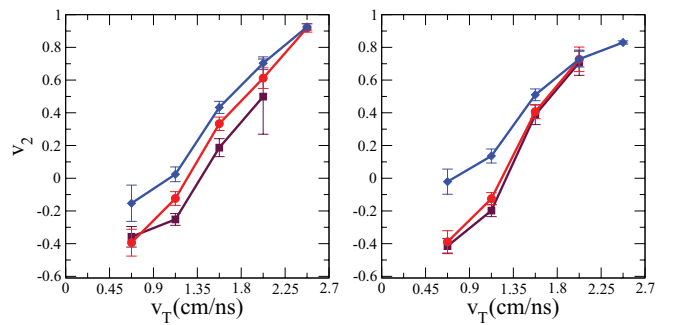


FIG. 11. (Color online) Elliptic flow anisotropy parameter  $v_2$  as a function of transverse velocity  $v_T$ . HH combination and events with three IMF's. Squares: heaviest IMF. Circles: second heaviest IMF. Diamonds: lightest IMF in the hierarchy. Left panel: asysoft EOS. Right panel: asysuperstiff EOS.

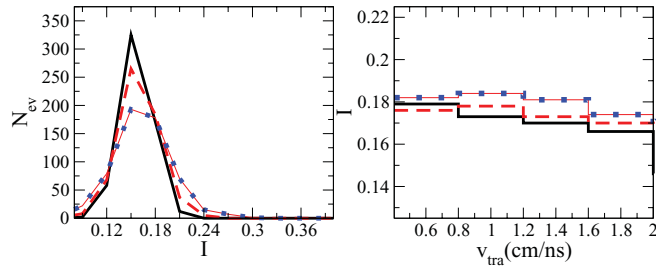


FIG. 12. (Color online) HH combination in the asysoft EOS choice. Events with three IMF's. Left panel: Isospin distribution. Right panel: Fragment isospin content as a function of transverse velocity. All lines are like in the caption of Fig. 4.

Fig. 8. All these features should be considered as specific to this fragmentation mechanism. We stress that some other production mechanisms are likely to exist, with properties differing from those evidenced above but not described by our transport model. These include breakup or fission of strongly deformed quasiprojectiles or quasitargets, which take place on longer time scales, as well as statistical decay of the primary fragments. However, it is hoped that a proper selection of kinematic characteristics can single out various classes of events.

#### IV. ISOSPIN EFFECTS

As already noted, the features discussed above are determined mainly by the isoscalar part of the equation of state. On top of that, the symmetry energy induces various changes on the properties related to the isospin content of the fragments. We have extended our investigations to isospin observables, studying their dependence on the IMF position in the hierarchy and their correlation to the transverse velocity. In Figs. 12 and 13 (for asysoft EOS) and 14 and 15 (for asysuperstiff EOS) we report the asymmetry  $I = (N - Z)/(N + Z)$  distribution of each IMF of the hierarchy. The results refer again to the HH system whose initial asymmetry is  $I = 0.194$ .

Several differences between the two asy-EOS are evidenced. For asysoft EOS the isospin distributions are centered at a lower value and their widths are rather narrow. At variance, for asysuperstiff EOS the centroids of the distributions are closer to the initial value of the composite system and their

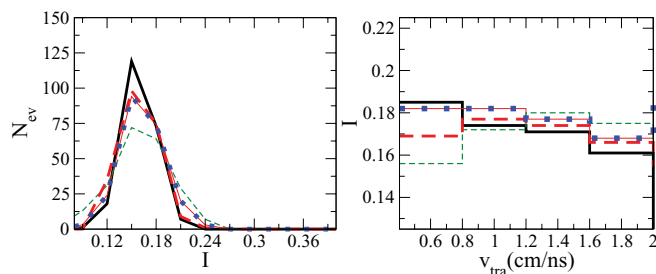


FIG. 13. (Color online) HH combination in the asysoft EOS choice. Events with four IMF's. Left panel: Isospin distribution. Right panel: Fragment isospin content as a function of transverse velocity. All lines are like in the caption of Fig. 5.

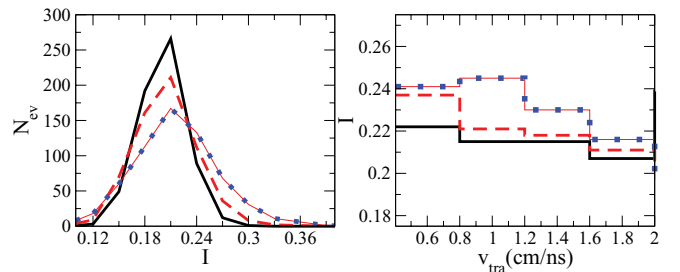


FIG. 14. (Color online) Like in Fig. 12, for the asysuperstiff EOS choice.

broader widths depend on the position in the mass hierarchy. For both asy-EOS the lightest IMF's are more likely to acquire higher values of the asymmetry. We also notice that similar results were obtained for the other entrance channel combination (LL).

The average asymmetry is represented as a function of the transverse velocity in the right panels of Figs. 12–15, for asysoft and asysuperstiff EOS choice, respectively. A decreasing trend is generally observed for the IMF's, more pronounced for the latter EOS. In this case, the trend is particularly evident for the lightest IMF's. These features can be related to the behavior of the symmetry energy at subsaturation densities and to the combined effect of the isospin distillation and migration mechanisms.

First, isospin migration is expected in neck fragmentation volume: the neutron excess is transferred from the PLF and TLF regions toward the low-density neck region. While fragments are formed, the neutron richness of the neck region increases with time. Hence, IMF's with large transverse velocity, that quickly leave the system, are more symmetric than slow fragments. This effect is particularly evident for light fragments and more for the case of the asysuperstiff interaction, for which the isospin migration mechanism is more efficient, corresponding to the larger derivative of the symmetry energy below normal density [1].

At the same time, along the fragment growth, the produced IMF's are becoming more symmetric than the matter initially located in the neck region, while the emitted light particles are more neutron rich (isospin distillation). Clearly, a larger value of the symmetry energy will fasten this process and all IMF's reach lower and closer values of the asymmetry. This is the case observed for the asysoft EOS. On the other hand, the larger

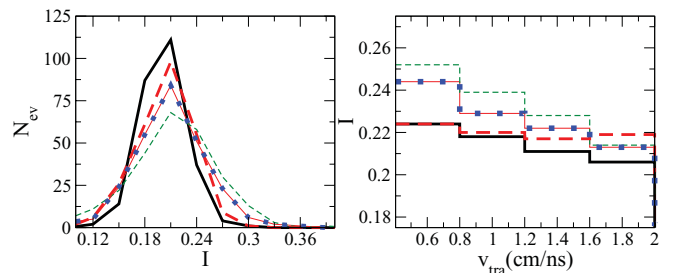


FIG. 15. (Color online) Like in Fig. 13, for the asysuperstiff EOS choice.

values of fragment asymmetry obtained for the asysuperstiff EOS indicate that the distillation mechanism was not very effective, owing to the small value of the symmetry energy below normal density.

The same type of analysis has been carried out for the LL combination, aiming to construct isotopic double ratios and to study their dependence on the transverse velocities. Concerning the fragment isotopic content, similar differences between the two asy-EOS, as observed for the HH combination, were evidenced, in spite of the fact that Coulomb effects are now more important. We also observed an analogous trend of the fragment asymmetry with the transverse velocity. Therefore, in this case, the double ratios do not show appreciable differences between the two asy-EOS. The same conclusion was reached in central collisions [28]. However, as we noticed before, differences can be evidenced even within the same system, by comparison between fragments belonging to different ranks in the hierarchy for appropriate kinematic selections.

## V. CONCLUSIONS AND PERSPECTIVES

In this paper, by employing a microscopic transport model, we unveiled new features of nuclear fragmentation in semi-central to semiperipheral collisions from the study of several kinematic correlations of intermediate mass fragments.

At Fermi energies, an almost continuous transition with the centrality, from multifragmentation to neck fragmentation mechanisms, is revealed. Good observable tracers appear to be related to the correlations between the fragment masses, transverse velocities, and isospin content. Specific hierarchy phenomena are signaled: the distributions of the velocity perpendicular to the intrinsic axis of the event depend on the rank in the mass hierarchy of the event. In the reaction plane the lightest fragments acquire greater transverse velocities, a phenomenon observed for several mass entrance channels. This feature can be used as an identification of the fragmentation mechanism discussed in this paper.

Another important finding is that the fragment isospin content is sensitive to the position in this hierarchy and the acquired transverse velocity. This behavior is mainly determined by the density dependence of the symmetry energy below saturation and depends on the relative time scales for fragment formation and isospin transport.

These observations open new opportunities from the experimental point of view. An analysis of isospin-dependent observables in correlation to position in the mass hierarchy and kinematic features may add other constraints upon the behavior of the symmetry energy below normal density and can provide a supplementary support for the assumption that the IMF's form in the low-density regions of heated nuclear matter. We mention that recent experimental results, reported by the CHIMERA collaboration for the system Sn + Ni at a lower energy (35A MeV) [42], sustain the existence of the hierarchy in transverse velocity, as discussed in this paper. Their analysis also signaled differences in the isospin content of the IMF's when ordered in a mass hierarchy, the lightest fragments being more asymmetric. This kind of observation supports an asystifflike behavior of the symmetry energy at subsaturation densities.

## ACKNOWLEDGMENTS

The authors are grateful to E. De Filippo, A. Pagano, P. Russotto, and the CHIMERA Collaboration for stimulating discussions. V. Baran is thankful for warm hospitality at Laboratori Nazionali del Sud. This work for V. Baran was supported by a grant of the Romanian National Authority for Scientific Research, Consiliul National al Cercetarii Stiintifice, Unitatea Executiva Pentru Finantarea Invatamantului Superior, a Cercetarii, Dezvoltarii si Inovarii, Project No. PN-II-ID-PCE-2011-3-0972. For R. Zus this work was supported by the strategic Grant No. POSDRU/89/1.5/S/58852, Project "Postdoctoral programme for training scientific researchers" co-financed by the European Social Found within the Sectorial Operational Program Human Resources Development 2007–2013.

- 
- [1] V. Baran, M. Colonna, M. Di Toro, and V. Greco, *Phys. Rep.* **410**, 335 (2005).
  - [2] A. W. Steiner, M. Prakash, J. M. Lattimer, and P. J. Ellis, *Phys. Rep.* **411**, 325 (2005).
  - [3] B.-A. Li, L.-W. Chen, and C.-M. Ko, *Phys. Rep.* **464**, 113 (2008).
  - [4] P. Chomaz, M. Colonna, and J. Randrup, *Phys. Rep.* **389**, 263 (2004).
  - [5] D. H. E. Gross, *Rep. Prog. Phys.* **53**, 605 (1990).
  - [6] J. P. Bondorf *et al.*, *Phys. Rep.* **257**, 133 (1995).
  - [7] D. H. E. Gross, *Phys. Rep.* **279**, 120 (1997).
  - [8] A. H. Raduta, M. Colonna, and M. Di Toro, *Phys. Rev. C* **76**, 024602 (2007).
  - [9] J. Frankland *et al.*, *Nucl. Phys. A* **689**, 940 (2001); B. Borderie *et al.*, *Phys. Rev. Lett.* **86**, 3252 (2001).
  - [10] V. Baran, M. Colonna, M. Di Toro, A. B. Larionov, *Nucl. Phys. A* **632**, 287 (1998).
  - [11] V. Baran, M. Colonna, M. Di Toro, and V. Greco, *Phys. Rev. Lett.* **86**, 4492 (2001).
  - [12] C. P. Montoya *et al.*, *Phys. Rev. Lett.* **73**, 3070 (1994).
  - [13] J. Toke *et al.*, *Phys. Rev. Lett.* **75**, 2920 (1995).
  - [14] P. Milazzo *et al.*, *Nucl. Phys. A* **703**, 466 (2002).
  - [15] E. De Filippo *et al.*, *Phys. Rev. C* **71**, 044602 (2005).
  - [16] M. Di Toro, A. Olmi, and R. Roy, *Eur. Phys. J. A* **30**, 65 (2006).
  - [17] P. Russotto *et al.* (Chimera Coll.), *Phys. Rev. C* **81**, 064605 (2010).
  - [18] V. Baran, M. Colonna, and M. Di Toro, *Nucl. Phys. A* **730**, 329 (2004).
  - [19] M. Papa *et al.*, *Phys. Rev. C* **75**, 054616 (2007).
  - [20] Y. Zhang *et al.*, *Phys. Rev. C* **85**, 024602 (2012).
  - [21] G. Casini *et al.*, *Phys. Rev. Lett.* **71**, 2567 (1993).
  - [22] E. De Filippo *et al.*, *Phys. Rev. C* **71**, 064604 (2005).
  - [23] P. Russotto *et al.* (Chimera Coll.), *Int. J. Mod. Phys. E* **15**, 410 (2006).
  - [24] M. B. Tsang *et al.*, *Phys. Rev. Lett.* **92**, 062701 (2004); X. Liu *et al.*, *Europhys. Lett.* **74**, 806 (2006); M. B. Tsang, Y. Zhang,

- P. Danielewicz, M. Famiano, Z. Li, W. G. Lynch, and A. W. Steiner, *Phys. Rev. Lett.* **102**, 122701 (2009).
- [25] V. Baran, M. Colonna, M. Di Toro, M. Zielinska-Pfabe, and H. H. Wolter, *Phys. Rev. C* **72**, 064620 (2005).
- [26] J. Rizzo *et al.*, *Nucl. Phys. A* **806**, 79 (2008).
- [27] D. D. S. Coupland, W. G. Lynch, M. B. Tsang, P. Danielewicz, and Y. Zhang, *Phys. Rev. C* **84**, 054603 (2011).
- [28] M. Colonna, V. Baran, M. Di Toro, and H. H. Wolter, *Phys. Rev. C* **78**, 064618 (2008).
- [29] J. Colin *et al.* (INDRA Coll.), *Phys. Rev. C* **67**, 064603 (2003).
- [30] A. B. McIntosh *et al.*, *Phys. Rev. C* **81**, 034603 (2010).
- [31] J. Rizzo, Ph. Chomaz, and M. Colonna, *Nucl. Phys. A* **806**, 40 (2008).
- [32] M. Colonna *et al.*, *Nucl. Phys. A* **642**, 449 (1998).
- [33] M. Colonna, M. Di Toro, G. Fabbri, and S. Maccarone, *Phys. Rev. C* **57**, 1410 (1998).
- [34] A. Guarnera, M. Colonna, and Ph. Chomaz, *Phys. Lett. B* **373**, 267 (1996).
- [35] V. Baran, B. Frecus, M. Colonna, and M. Di Toro, *Phys. Rev. C* **85**, 051601(R) (2012).
- [36] N. Paar, T. Nicsik, D. Vretenar, and P. Ring, *Phys. Lett. B* **606**, 288 (2005).
- [37] V. Baran *et al.*, *Nucl. Phys. A* **703**, 603 (2002).
- [38] A. A. Stefanini *et al.*, *Z. Phys. A* **351**, 167 (1995).
- [39] J. Wilczynski *et al.* (CHIMERA Coll.), *Int. J. Mod. Phys. E* **14**, 353 (2005).
- [40] R. Lioni, V. Baran, M. Colonna, and M. Di Toro, *Phys. Lett. B* **625**, 33 (2005).
- [41] J. D. Frankland *et al.*, *Nucl. Phys. A* **689**, 940 (2001); M. Colonna, A. Ono, and J. Rizzo, *Phys. Rev. C* **82**, 054613 (2010).
- [42] E. De Filippo *et al.* (CHIMERA Coll.), *Conference Proceedings of IWM2009-International Workshop on Multifragmentation and Related topics*, edited by J. D. Frankland, A. Pagano, S. Pirrone, M-F Rivet and F. Rizzo, (Società Italiana di Fisica (SIF), Bologna, 2010), Vol. 101, pp. 178–188; E. De Filippo and P. Russotto (private communication).